Int. J. Electrochem. Sci., 12 **(2017)** 6393 – 6403, doi: 10.20964/2017.07.51

International Journal of
ELECTROCHEMICAL
SCIENCE
www.electrochemsci.org

Electrochemistry of Zirconium in Molten Chlorides

Liang Xu[1], *Yanping Xiao*[3], *Qian Xu*[2,*], *Qiushi Song*[1], *Yongxiang Yang*[3,4]

[1] School of Metallurgy, Northeastern University, Shenyang 110004, China
[2] State Key Laboratory of Advanced Special Steel, Shanghai University, Shanghai 200072, China
[3] School of Metallurgical Engineering, Anhui University of Technology, Ma'anshan 243002, China
[4] Department of Materials Science and Engineering, Delft University of Technology, 2628 CD Delft, The Netherlands
[*]E-mail: qianxu@shu.edu.cn

Received: 5 April 2017 / *Accepted:* 29 April 2017 / *Published:* 12 June 2017

In this work, the electrochemical behavior of zirconium was studied on an inert molybdenum electrode at 550 °C in a LiCl-KCl-K_2ZrF_6 molten salt system, which is considered as an ideal electrolyte for the zirconium electrorefining process. Several transient electrochemical techniques were used such as cyclic voltammetry, chronopotentiometry, square wave voltammetry, and open circuit chronopotentiometry. The reduction of Zr (IV) was determined to follow a two-step mechanism of Zr (IV)/Zr (II) and Zr (II)/Zr. The diffusion coefficient of Zr (IV) was investigated with cyclic voltammetry and chronopotentiometry, and the results turned out to be in fair agreement from the both methods, as to be 4.26×10^{-5} and 4.98×10^{-5} cm^2/s, respectively. The present study aims to provide a theoretical reference for the Zr electrorefining process.

Keywords: redox mechanism, zirconium, molten salt, electrochemistry.

1. INTRODUCTION

Zirconium is an irreplaceable material in nuclear reactors for structural purposes and for containing nuclear fuels due to its extremely low neutron-capture cross-section [1]. The Zr cladding can be contaminated by the penetration of fission products and transuranic elements after long time use and lose the excellent nuclear properties [2]. Therefore, the recovery of Zr from contaminated Zr alloy scraps has been a research topic for decades in nuclear industry.

Pyroprocessing is a promising option for recycling and treating spent Zr alloys since it has benefits in terms of economic advantage and environmental safety. The molten salt electrorefining process is the key step of the pyrometallurgical route, which is able to effectively produce refractory

metals and their alloys, and has been developed as an effective method for high purity Zr recovery from Zr alloy scraps [3, 4].

For the Zr electrorefining process, the highly pure metallic Zr is selectively deposited on the cathode from the anode of Zr alloy scraps in the molten salt by applying an appropriate voltage/current density. In order to improve the efficiency and reliability of the electrolytic process, it is critical to comprehend the precise knowledge of redox behavior of Zr in the molten salt. So far, a number of investigations have been performed on Zr electrochemistry in chloride-based mediums such as LiCl-KCl-$ZrCl_4$ [2, 3, 5-8], NaCl-$ZrCl_4$ [9], and NaCl-KCl-ZrF_4 [10] and -K_2ZrF_6 [11], for the reason of low-temperature operation. For the purpose of decreasing the hygroscopicity and volatility of the molten baths [12], a few studies have been carried out in fluoride salt systems, such as LiF-NaF-KF (known as FLINAK) -ZrF_4 [13] and –K_2ZrF_6 [14], LiF-CaF_2-ZrF_4 [15], and LiF-KF-ZrF_4 [4, 16]. However, electrolysis in fluoride baths normally requires the operation temperatures of approximately 200 °C higher than that in chloride baths, which will consume much more energy and generate severe corrosion issue in the industrial-scale electrolytic cell.

From the literature survey [2-16], several oxidation states of 0, +I, +II, and +IV for Zr either in chloride or in fluoride salt system have been reported, but no consensus on the redox mechanism among these states has been found yet due to different experimental conditions of operation temperature, electrode material, salt composition and Zr ions concentration in the melt. The disagreement over explanations on Zr electrochemical behavior suggests that further investigation on Zr electrochemistry in molten salt is indispensable.

In the present study, the reduction/oxidation mechanisms of Zr was investigated in the LiCl-KCl eutectic melt which is considered as the ideal supporting electrolyte for the electrorefining process due to its low melting point and excellent conductivity. K_2ZrF_6 was selected as the Zr ions source because of the much lower price compared to ZrF_4 and better stability than that of $ZrCl_4$ at high temperature. Transient electrochemical techniques of cyclic voltammetry, chronopotentiometry, square wave voltammetry, as well as open circuit chronopotentiometry were applied to investigate the typical redox potentials of Zr, reversibility of the electrode reactions, and diffusion coefficient of Zr ions in the molten melt. The present study aims to provide a theoretical reference for the Zr electrorefining from Zr alloy scraps in the molten salt.

2. EXPERIMENTAL

All the electrochemical experiments were carried out in a three-electrode system assembled in a corundum crucible, which was placed within the constant temperature zone of a stainless steel vessel and heated in an electric furnace. The experimental set-up used in this work was described in detail in the previous publication of our group [16]. The temperature in the experiment was measured with a Chromel-Alumel thermocouple with an accuracy of ±2 °C and maintained at 550 °C by a proportional-integral-derivative (PDI) thermal controller. The inert experimental atmosphere was achieved with continuous argon gas circulation of 99.999% purity.

All the potentials in this work were measured with respect to an Ag/AgCl (1.0%) reference electrode, which was self-assembled in a round bottom mullite tube. A molybdenum wire (1 mm diameter, 99.95% purity) was served as the working electrode, and a graphite rod (6 mm diameter, spectroscopically pure) was used as the counter electrode. The electrodes were cleaned by polishing with fine abrasive paper and washing ultrasonically in distilled water and anhydrous ethanol before using.

All the chemical reagents employed in this study were of analytical grade. The mixture of LiCl-KCl with eutectic composition (59:41 mol%) was served as supporting electrolyte, previously dehydrated at 300°C for 72 h and pre-melted at 550°C for the removal of residual moisture. The pre-melted salt mixture was melted again at 550°C for the main experiments. Pre-electrolysis was performed with the applied voltage of 2.8 V between two graphite rods for 2 h to remove residual impurities in the system. Zirconium ions were introduced into the melt in the form of K_2ZrF_6 (1 wt%). The electrodes were inserted in the molten melt with an immersion area of 0.4788 cm^2 for the working electrode, and sufficient equilibrium between the electrodes and the molten salt was guaranteed by immersing the electrodes in the melt for more than 2 h before the electrochemical measurements.

All the electrochemical measurements were carried out with the AUTOLAB/PGSTAT320 potentiostat from M/s. EcoChemie, the Netherlands. The data acquisition was conducted with GPES 4.9 software. The transient electrochemical techniques of cyclic voltammetry, chronopotentiometry, square wave voltammetry, and open circuit chronopotentiometry were used to study the electrochemical behavior of Zr in the molten salt.

3. RESULTS AND DISCUSSION

3.1 Cyclic voltammetry in LiCl-KCl with/without addition of Zr ions

Cyclic voltammograms in molten LiCl-KCl and in LiCl-KCl-K_2ZrF_6 (1 wt%) systems with the scan rate of 100 mV/s for a molybdenum electrode at 550 °C were recorded in Fig. 1. The CV curve of the blank LiCl-KCl eutectic represented in Fig. 1 inset delivered one redox couple of R_0 and O_0 over the potential range of 0 to -2.5 V, which are known as to be due to the deposition and dissolution of Li, respectively [8, 17]. No more redox peaks were found within this range, suggesting that the effects of impurities in the supporting electrolyte are negligible for all the electrochemical measurements.

With the presence of Zr ions in the molten melt, the recorded CV curve clearly showed two cathodic peaks of R_1 and R_2 at -1.05 and -1.30 V, respectively, and their corresponding anodic peaks of O_1 and O_2 were observed at -0.90 and -0.85 V, respectively, when the potential was swept back to positive side. Peak O_2 is hidden by O_1 due to the high peak current of O_1. The multiple current peaks observed in the CV measurement indicate the multi-step redox mechanism of zirconium in LiCl-KCl.

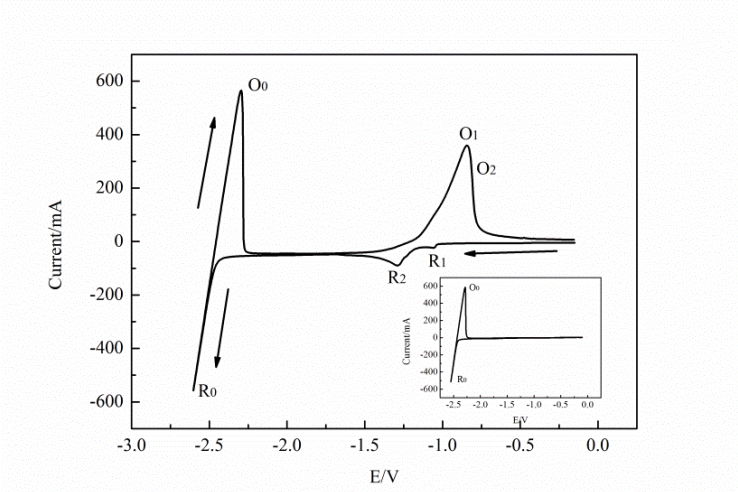

Figure 1. Cyclic voltammogram of the LiCl-KCl-K_2ZrF_6 (1 wt%) system at 550 °C with the scan rate of 100 mV/s. Inset: Cyclic voltammogram of the blank LiF-NaF eutectic melt.

3.2 Cyclic voltammetry with varied scan ranges

A set of CV measurements in the molten LiCl-KCl-K_2ZrF_6 melt with a scan rate of 100 mV/s were conducted for seven different scan ranges, and the results are shown in Fig. 2. It can be seen that no current peaks were observed in the potential range of -0.1 to -1.0 V, indicating no reduction/oxidation reaction occurred in this range. When the scan range was expanded to -1.1 V, the reduction peak R_1 appeared in the CV curve and its corresponding oxidation peak O_2 was evident subsequently during the anodic scanning process. This redox couple is attributed to the soluble-soluble reactions involving Zr (II) and Zr (IV) ions, which are known as stable species in the LiCl-KCl system [8, 18]. The redox reactions for peaks R_1 and O_2 are represented in Eqs. (1) and (2). This couple of redox reactions are expected to proceed slowly due to the low peak currents, which is mainly attributed to the small exchange current density in Butler-Volmer kinetics [2].

Peak R_1: $\mathrm{Zr(IV) + 2e \rightarrow Zr(II)}$ (1)

Peak O_2: $\mathrm{Zr(II) \rightarrow Zr(IV) + 2e}$ (2)

When the potential was swept over -1.2 V, the cathodic peak R_2 and its corresponding anodic peaks O_1 started to appear and the peaks turned out to be more and more identified as the expansion of potential range. The peak shape of O_2 was hard to be identified since peak O_1 was intensified when the scan range was extended to -1.6 V. The cathodic peak R_2 is believed to be associated with the formation of metallic Zr, mainly reduced from Zr (II) ions, and the anodic peaks O_1 should be corresponded to R_2, representing the oxidation process of Zr to Zr (II). The electrochemical reactions for the redox couple of R_2 and O_1 are illustrated in Eqs. (3) and (4), respectively.

Peak R_2: $\mathrm{Zr(II) + 2e \rightarrow Zr}$ (3)

Peak O_1: $Zr \rightarrow Zr(II) + 2e$ (4)

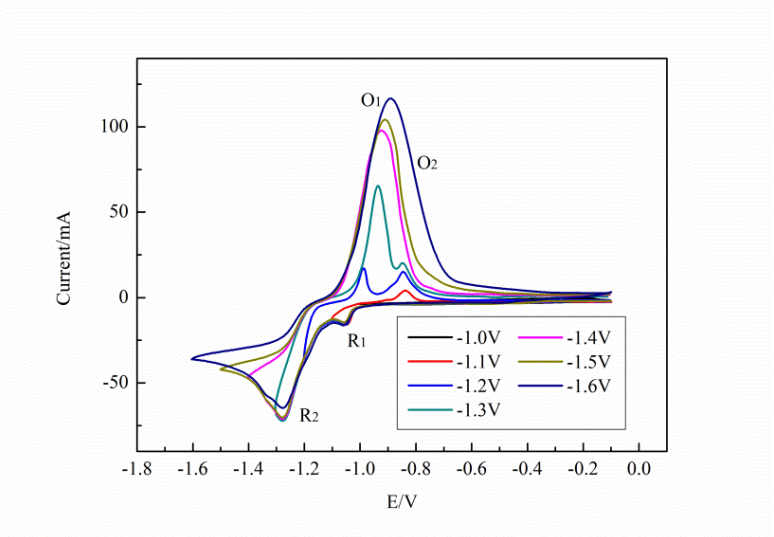

Figure 2. Cyclic voltammograms of the LiCl-KCl-K_2ZrF_6 (1 wt%) system at 550 °C with the scan rate of 100 mV/s in varied scan ranges.

3.3 Cyclic voltammetry with varied scan rates

Cyclic voltammograms of the LiCl-KCl-K_2ZrF_6 (1 wt%) melt with a fixed potential range from 0.0 to -1.7 V at varied scan rates are shown in Fig. 3. It is clear that the redox peaks R_1, R_2 and O_1 are well evident in the CV curves, whereas the peak shape of O_2 is less prominent since it is hidden by peak O_1. In general, the peak currents of the redox peaks increased with increasing the scan rate. For the cathodic process, the peak potentials of R_1 and R_2 moved to negative side with the potential changes of 29 and 68 mV respectively, when the scan rate was increased from 100 to 1300 mV/s.

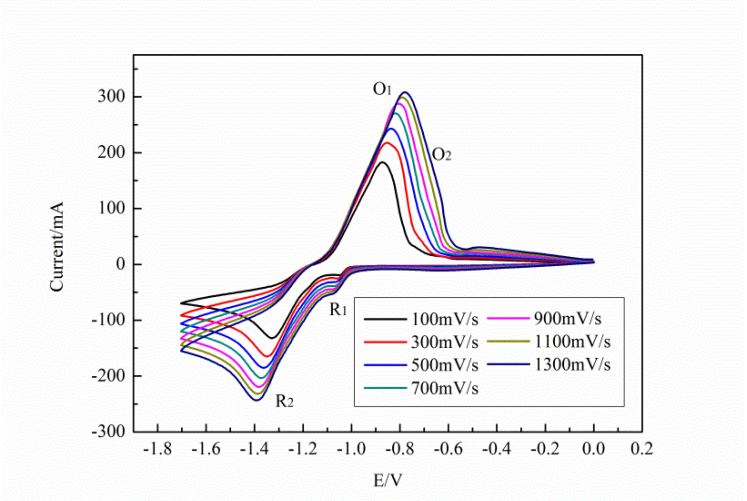

Figure 3. Cyclic voltammograms of the LiCl-KCl-K_2ZrF_6 (1 wt%) system with varied scan rates at 550 °C.

The relationship between scan rate and peak potential/current for the cathodic reactions is shown in Fig. 4. It can be seen from Fig. 4 (a) that the shift of peak potential for the electrode reaction

either at R_1 or R_2 was small with the increase of scan rate from 100 to 1300 mV/s, which indicates the reversibility of the both cathodic reactions. Moreover, the linear dependence of peak currents of R_1 and R_2 on the square root of the scan rates represented in Fig. 4 (b) reflects a diffusion-controlled mass transfer for the cathodic process.

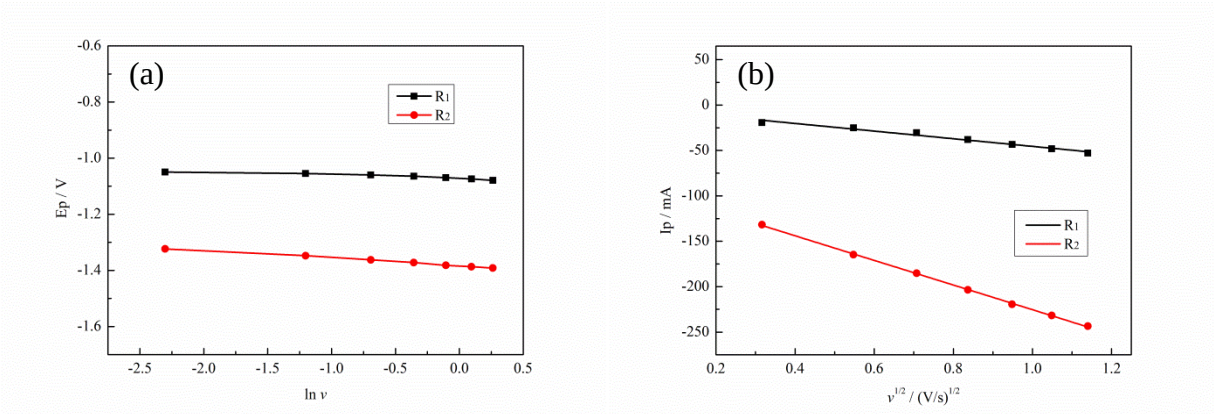

Figure 4. (a) Dependence of peak potential on natural logarithm of scan rate, (b) dependence of peak current on square root of scan rate.

For diffusion-controlled electrochemical reactions of reversibility, the diffusion coefficient of Zr ions in the molten salt can be estimated with the Randles-Shevchik equation, as shown in Eq. (5) [19].

$$i_p = 0.4463(nF)^{3/2}(RT)^{-1/2}AD^{1/2}Cv^{1/2} \quad (5)$$

Where A is the immersion area of the Mo working electrode (cm^2), n is the number of exchanged electrons, F is the Faraday constant (96485 C/mol), R is the molar gas constant (8.314 J/mol·K), T is the temperature (K), D is the diffusion coefficient of Zr ions (cm^2/s), C is the molar concentration of Zr ions (mol/cm^3), and *v* is the scan rate (V/s).

According to the relationship of diffusion coefficient with the peak currents at varied scan rates, the diffusion coefficient of Zr (IV) ions in the molten LiCl-KCl-K_2ZrF_6 (1 wt%) system at 550 °C was evaluated based on Eq. (5), as to be within the range of 1.64×10^{-5} and 6.89×10^{-5} cm^2/s, resulting in a mean value of 4.26×10^{-5} cm^2/s.

Moreover, the number of exchanged electrons for the cathodic process can be calculated according to Eq. (6), which is valid for the electrochemical reactions of reversibility [20].

$$E_p - E_{p/2} = 2.2\frac{RT}{nF} \quad (6)$$

Where E_p is the peak potential, and $E_{p/2}$ represents the half-peak potential.

In this study, the number of transferred electrons was estimated for the cathodic process at R_2 since the peak shape of R_1 is much less prominent. The n value for R_2 was evaluated at varied scan

rates of 100, 300, 500, 700, 900, 1100, and 1300 mV/s, and the corresponding results were turned out to be 2.07, 1.98, 1.95, 1.91, 1.88, 1.87, and 1.84, respectively, resulting in an average value of 1.93. The calculated data for n is in consistence with the cathodic mechanism concluded in section 3.2 that the electrochemical process at peak R_2 mainly involves the reduction of Zr (II) to Zr transferring two electrons, as illustrated in Eq. (3).

3.4 Chronopotentiometry

Typical chronopotentiograms with various applied current densities on the Mo electrode at 550 °C are shown in Fig. 5. The chronopotentiograms at low electrode currents of -10 to -20 mA represented in Fig. 5 (a) exhibit a transition time plateau at about -1.05 V, which is mainly due to the reduction of Zr (IV) to Zr (II) ions as concluded previously in the cyclic voltammetry analysis. In the case of high applied current densities, the plateau at approximately -1.30 V due to the Zr (II)/Zr couple is clearly evident in the chronopotentiograms, which completely masked the plateau for Zr (IV)/Zr (II) couple appeared at low current densities, as can be seen in Fig. 5 (b).

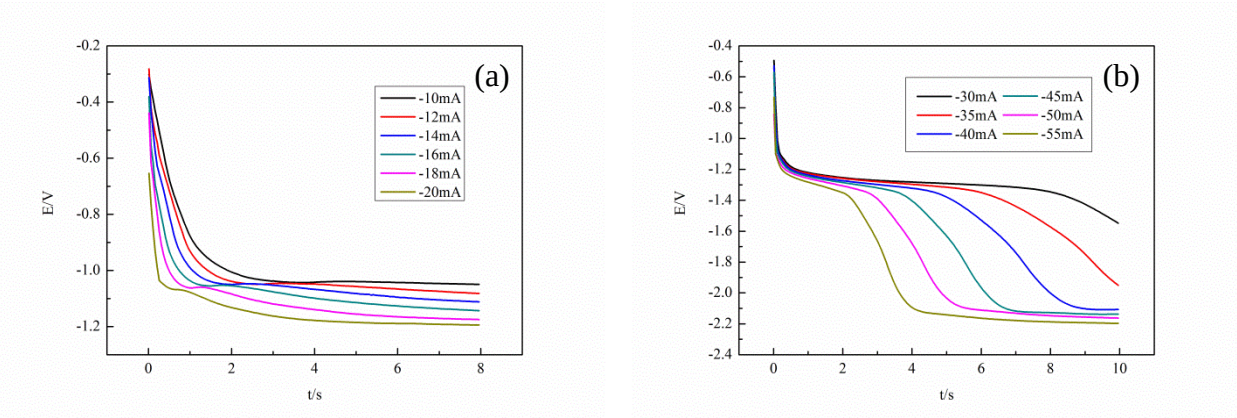

Figure 5. Chronopotentiograms of the LiCl-KCl-K_2ZrF_6 (1 wt%) system at 550 °C with varied applied current densities.

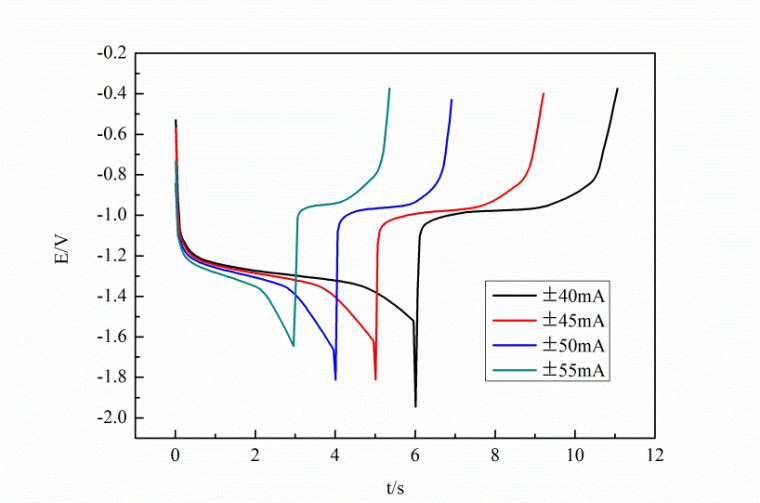

Figure 6. Current reversal chronopotentiograms of the LiCl-KCl-K_2ZrF_6 (1 wt%) system at 550 °C with varied applied current densities.

The plateau evidenced at much more negative potential region represents the reduction of Li. In general, the transition time decreased with the increase of the applied electrode current densities, which further confirms the reduction of zirconium is a diffusion-controlled process. The time-current relationship for a diffusion-controlled electron transfer process is given by the Sand's law for the purpose of diffusion coefficient evaluation for Zr ions in the melt, as seen in Eq. (7) [19].

$$i\tau^{1/2} = 0.5nFCA(\pi D)^{1/2} \quad (7)$$

The diffusion coefficient of Zr (IV) in the LiCl-KCl eutectic melt at 550 °C evaluated with Eq. (7) was turned out to be between 1.18×10^{-5} and 8.77×10^{-5} cm^2/s with an average value of 4.98×10^{-5} cm^2/s, which agrees well with the data obtained by cyclic voltammetries as summarized in section 3.3. Moreover, the diffusion coefficient of Zr (IV) ions evaluated in the present study accords closely with the corresponding results estimated by Yamada et al. of about 1.13×10^{-5} cm^2/s [21], Park et al. of 1.63×10^{-5} cm^2/s [2], Lee et al. of 7.77×10^{-5} cm^2/s [3], and Fabian et al. of approximately 1.50×10^{-5} cm^2/s [22] in the molten LiCl-KCl eutectic at 500 °C with experimental and computational methods.

Fig. 6 shows the current reversal chronopotentiograms for the molybdenum electrode at various applied current densities. It is seen that an anodic plateau in corresponding to the cathodic one is clearly identified after the current reversal for each applied current density on the electrode, and both of the anodic and cathodic transition time is determined to be almost equal to each other, as to be approximately 4.4, 3.7, 2.7, and 2.0 s with the electrode current of ±40, ±45, ±50, and ±55 mA, respectively. The equality of transition time indicates the deposition and dissolution of an insoluble compound during the cathodic and anodic processes, which further confirms that the metallic Zr was formed on the electrode through the reduction reaction of Zr (II)/Zr at about -1.30 V, as illustrated in Eq. (3).

3.5 Square wave voltammetry

A more sensitive transient electrochemical technique of square wave voltammetry [17, 23] was carried out to further investigate the electrochemical behavior of zirconium in the LiCl-KCl eutectic with the emphasis on the reduction process of Zr (IV). Fig. 7 shows a set of the typical square wave voltammograms of the LiCl-KCl-K_2ZrF_6 (1 wt%) system with the signal frequencies varying from 20 to 40 Hz. It is seen that the current peaks for R_1 and R_2 were well identified in the voltammograms, which are attributed to the multi-step reduction process of Zr (IV). Eq. (8) gives the relationship between the half-width of the peak and the number of transferred electrons for n values estimation, which is valid for reversible electrochemical systems.

$$W_{1/2} = 3.52\frac{RT}{nF} \quad (8)$$

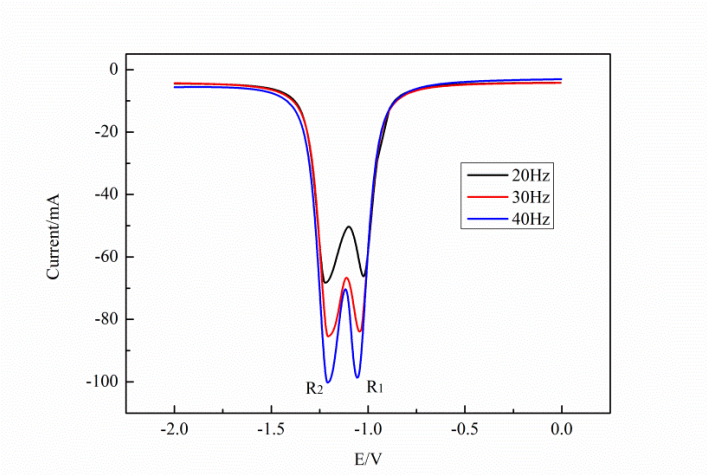

Figure 7. Square wave voltammograms of the LiCl-KCl-K_2ZrF_6 (1 wt%) system at 550 °C with varied signal frequencies.

It can be seen from Fig. 7 that the peak shapes of R_1 and R_2 are not symmetrical in nature. Similar phenomena have been reported previously for U (III) and Nd (III) by Taxil et al. [24, 25], Er (III) by Castrillejo et al. [26], and Zr (IV) by Ghosh et al. [8], and the reason was considered to be the change of the electrode surface state during the electrochemical process. The way of the measurement of $W_{1/2}$ data for the current peaks of asymmetry has been illustrated in detail in literature [25]. The numbers of transferred electrons evaluated based on Eq. (8) at the signal frequencies of 20, 30, and 40 Hz were turned out to be 2.12, 2.04, and 1.95, respectively, for R_1, and 2.21, 2.16, and 2.04, respectively, for R_2. The results delivered average n values of 2.04 and 2.13 for R_1 and R_2 respectively, confirming that the reduction of Zr (IV) follows a two-step mechanism of Zr (IV)/Zr(II) and Zr (II)/Zr, as concluded in the CV analysis.

3.6 Open circuit chronopotentiometry

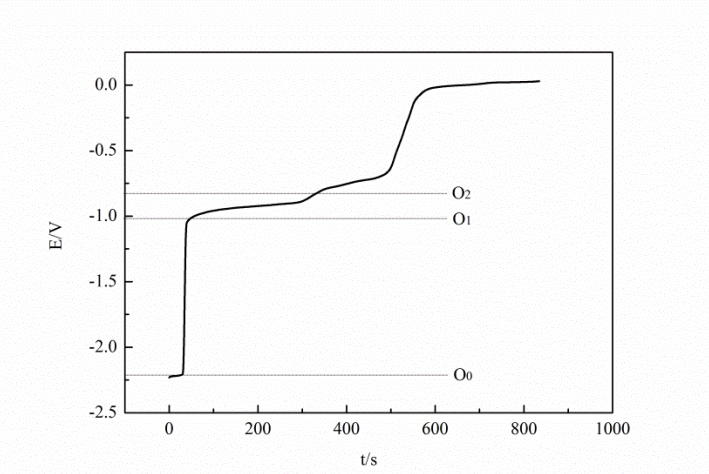

Figure 8. Open circuit chronopotentiogram of the LiCl-KCl-K_2ZrF_6 (1 wt%) system at 550 °C after electrochemical depositing at -2.5 V for 5 s on the Mo electrode.

Open circuit chronopotentiometry was carried out to comprehend the oxidation mechanism of zirconium in the molten LiCl-KCl eutectic. The metallic Zr was first deposited on the molybdenum electrode at -2.5 V for 5 s and then the electrochemical control was switched off. The open circuit potential of the working electrode was recorded as a function of time as shown in Fig. 8. The first anodic plateau was evidenced at around -2.2 V, which is attributed to the dissolution of Li. The subsequent plateaus identified at about -1.0 and -0.8 V are corresponded to the two-step oxidation process of zirconium, associating with the couples of Zr/Zr (II) and Zr (II)/Zr (IV).

4. CONCLUSIONS

The present study examined the redox mechanism of zirconium in a molten LiCl-KCl-K_2ZrF_6 system on an inert molybdenum electrode at 550 °C with several transient electrochemical techniques of cyclic voltammetry, chronopotentiometry, square wave voltammetry, and open circuit chronopotentiometry. The reduction of Zr (IV) was found to be a two-step process of Zr (IV)/Zr (II) and Zr (II)/Zr. This cathodic mechanism was further confirmed by the theoretical evaluation of number of transferred electrons through cyclic voltammetry and square wave voltammetry analysis. The diffusion coefficient of Zr (IV) in the melt was determined to be about 4.26×10^{-5} cm^2/s by cyclic voltammetry, and approximately 4.98×10^{-5} cm^2/s through chronopotentiometry. The results obtained by both the methods are in good agreement.

ACKNOWLEDGEMENTS
The authors acknowledge the financial support of the National Natural Science Foundation of China (NSFC) Grant No. 51274005 and 51174055.

References

1. L. Xu, Y. Xiao, A. van Sandwijk, Q. Xu and Y. Yang, *J. Nucl. Mater.*, 466 (2015) 21.
2. J. Park, S. Choi, S. Sohn, K. Kim and I. S. Hwang, *J. Electrochem. Soc.*, 161 (2014) H97.
3. C. H. Lee, K. H. Kang, M. K. Jeon, C. M. Heo and Y. L. Lee, *J. Electrochem. Soc.*, 159 (2012) D463.
4. K. T. Park, T. H. Lee, N. C. Jo, H. H. Nersisyan, B. S. Chun, H. H. Lee and J. H. Lee, *J. Nucl. Mater.*, 436 (2013) 130.
5. T. Murakami and T. Kato, *J. Electrochem. Soc.*, 155 (2008) E90.
6. Y. Sakamura, *J. Electrochem. Soc.*, 151 (2004) C187.
7. Y. Cai, H. Liu, Q. Xu, Q. Song and L. Xu, *Electrochim. Acta*, 161 (2015) 177.
8. S. Ghosh, S. Vandarkuzhali, P. Venkatesh, G. Seenivasan, T. Subramanian, B. P. Reddy and K. Nagarajan, *J. Electroanal. Chem.*, 627 (2009) 15.
9. F. Basile, E. Chassaing and G. Lorthioir, *J. Appl. Electrochem.*, 11 (1981) 645.
10. F. Basile, E. Chassaing and G. Lorthioir, *J. Appl. Electrochem.*, 14 (1984) 731.
11. Y. Wu, Z. Xu, S. Chen, L. Wang and G. Li, *Rare Metals*, 30 (2011) 8.
12. H.A. Wilhelm and K.A. Walsh, *US Patent 2602725* (1952).
13. G. Mellors and S. Senderoff, *J. Electrochem. Soc.*, 113 (1966) 60.
14. G. Kipouros and S. Flengas, *J. Electrochem. Soc.*, 132 (1985) 1087.
15. M. Gibilaro, L. Massot, P. Chamelot, L. Cassayre and P. Taxil, *Electrochim. Acta*, 95 (2013) 185.

16. L. Xu, Y. Xiao, Q. Xu, A. van Sandwijk, J. Li, Z. Zhao, Q. Song and Y. Yang, *RSC Adv.*, 8 (2016) 84472.
17. H. Tang, Y. Yan, M. Zhang, X. Li, Y. Huang, Y. Xu, Y. Xue, W. Han and Z. Zhang, *Electrochim. Acta*, 88 (2013) 457.
18. S. Li, T. A. Johnson, B. R. Westphal, K. M. Goff and R. W. Benedict, Electrorefining experience for pyrochemical processing of spent EBR-II driver fuel, GLOBAL 2005, Tsukuba, Japan, 2005, 487.
19. A. J. Bard and L. R. Faulkner, Electrochemical methods: fundamentals and applications, John Wiley & Sons Inc, (2001) New York, America.
20. R. S. Nicholson and I. Shain, *Anal. Chem.*, 36 (1964) 706.
21. D. Yamada, T. Murai, K. Moritani, T. Sasaki, I. Takagi, H. Moriyama, K. Kinoshita and H. Yamana, *J. Alloys Compd.*, 444-445 (2007) 557.
22. C. P. Fabian, V. Luca, T. H. Le, A. M. Bond, P. Chamelot, L. Massot, C. Caravaca, T. L. Hanley and G. R. Lumpkin, *J. Electrochem. Soc.*, 160 (2013) H81.
23. K. Liu, Y. Liu, L. Yuan, X. Zhao, Z. Chai and W. Shi, *Electrochim. Acta*, 109 (2013) 732.
24. K. Serrano and P. Taxil, *J. Appl. Electrochem.*, 29 (1999) 497.
25. C. Hamel, P. Chamelot and P. Taxil, *Electrochim. Acta*, 49 (2004) 4467.
26. Y. Castrillejo, M. R. Bermejo, E. Barrado and A. M. Martinez, *Electrochim. Acta*, 51 (2006) 1941.